The Dynamics of a Packed Gas Absorber by Frequency Response Analysis

ROBERT I. GRAY and JOHN W. PRADOS

The University of Tennessee, Knoxville, Tennessee

The unsteady state behavior of a packed-column gas absorber was investigated by comparing the results of experimental frequency response tests with theoretical frequency responses determined for several postulated flow models.

Carbon dioxide was absorbed in water from air-carbon dioxide mixtures in a 6-in. I.D. Pyrex pipe, packed to a depth of 5.12 ft. with ⅝-in. ceramic Raschig rings. A sinusoidal variation in inlet gas-phase carbon dioxide concentration was produced by a specially designed linear valve, driven at frequencies of 0.1 to 15 cycles/min. Inlet and outlet gas-phase concentration sinusoids were measured continuously with specially designed high-speed thermal conductivity cells. Liquid flows from 0 to 222 lb. moles/hr.-sq. ft. and gas flows from 1 to 20 lb. moles/hr.-sq. ft. were investigated. Separate frequency response tests on inlet and outlet mock-ups permitted determination of the frequency response of the packing section alone. Results were expressed graphically as Bode plots.

Theoretical frequency response curves were calculated based on three different flow models: no axial mixing, axial mixing described by a series of perfectly mixed cells, and axial mixing described by an effective longitudinal diffusivity. Neither of the three models gave completely satisfactory agreement with the experimental magnitude-ratio curves above about 1 cycle/min., although the slug flow model appeared somewhat better than the others. The theoretical phase-shift curves were almost indistinguishable for the three models and agreed well with the experimental curves.

Since 1954 an increasing number of studies of the dynamic behavior of chemical engineering equipment have appeared in the literature (*1, 2, 3, 4, 5, 6*). Noticeably absent however have been significant investigations of continuous countercurrent diffusional operations in packed and spray columns. Equations describing the dynamics of such operations have been presented and solutions obtained for special cases (*7, 8*); however no corresponding experimental studies have been reported. The present paper describes an experimental investigation of the dynamics of a packed gas absorber. The frequency response technique was chosen, as results obtained by this method are usually highly reproducible and are relatively easy to compare with predictions from theoretical models.

In frequency response experiments a measured system input variable is caused to vary sinusoidally with time. For a linear system the measured output variable will, after an initial transient has decayed, also vary sinusoidally with the same frequency as the input but with a different amplitude and phase relation. The dynamic characteristics of the system can be described in terms of the ratio of output to input amplitudes, the amplitude ratio, and the phase shift, or angular displacement between the two waves. The frequency response method has been applied in a number of dynamic studies of chemical process equipment, including stirred tank reactors (*9, 10*), heat exchangers (*6, 11, 12*), a spray dryer (*11*), turbulent flow system (*13, 14*), bubble cap plates (*15*), and packed beds (*3, 16, 17, 18*).

A major deterrent to experimental studies of mass transport dynamics has been the lack of a satisfactory method for continuous measurement of rapidly changing liquid- or gas-phase compositions. In the present study electrical conductivity (*2, 17*), continuous photometry (*16, 19*), mass spectroscopy (*20*), and α-ionization (*3, 21, 22, 23*) were considered and rejected for reasons of cost or experimental difficulty. Thermal conductivity analysis was the final choice. Although the method, as used commercially, is very slow, and although its previous use in frequency response experiments created significant experimental difficulties (*13*), it was believed that considerable improvement could be made in the design and application of the equipment.

The system carbon dioxide-air-water was selected for the absorption experiments, primarily for the ready availability, low cost, and ease of handling of these components. Furthermore carbon dioxide-air mixtures are well suited for thermal conductivity analysis. A disadvantage of the system was the relative insolubility of the carbon dioxide, necessitating large L/G ratios in order to obtain significant absorption rates.

THEORETICAL MODELS

Theoretical responses (amplitude ratios and phase shifts) for the absorption process were calculated for three flow models, which differ only in the manner by which the process of axial dispersion, or mixing of mass along the column length, is described. These are referred to as the *slug flow, mixing cell,* and *axial diffusion* models. In the slug flow model it is assumed that there is no axial mixing whatever, implying that both phases are completely mixed in the radial direction and have flat velocity profiles. This latter condition is frequently not satisfied (*24*). In the mixing cell and axial diffusion models one attempts to account for the longitudinal mixing by assuming that the system acts as a series of noninteracting, perfect mixers or that the axial mixing can be described by a Fickian diffusion term, respectively.

Slug Flow Model

For slug flow, conservation of solute component in the liquid and gas phase for an incremental packing height dz leads to the following equations under the assumptions that holdups and flow rates are constant;

$$L\frac{\partial x}{\partial z} + Ra = h_L\frac{\partial x}{\partial t} \qquad (1)$$

$$G\frac{\partial y}{\partial z} + Ra = -h_a\frac{\partial y}{\partial t} \qquad (2)$$

For the carbon dioxide-water system physical absorption is controlled by the liquid side resistance. The mass transfer rate equation can be written as

$$Ra = k_L a(x^* - x) \qquad (3)$$

and the equilibrium follows a linear relation

$$y = mx^* \qquad (4)$$

Theoretical frequency response functions for this model are calculated by application of the Laplace transformation to Equations (1) to (4) and appropriate substitution of the results to form an ordinary, second-order differential equation in the transformed gas-phase composition $\bar{y}(z)$. By choosing the composition scales so that all composition variables were measured from their original steady state values, initial conditions were made equal to zero. Solution of the differential equations for $\bar{y}(z)$, subject to the boundary

Robert I. Gray is now with the Union Carbide Chemicals Company, South Charleston, West Virginia.

conditions $\bar{y} = \bar{y}(0)$ at $z = 0$; $\bar{x} = 0$ at $z = Z$, yields the system transfer function

$$\frac{\bar{y}(Z)}{\bar{y}(0)} = \frac{p_2 - p_1}{(q - p_1)\exp(-p_1 Z) - (q - p_2)\exp(-p_2 Z)} \quad (5)$$

where

$$p_{1,2} = \frac{(d + cs) \pm \sqrt{(c^2 + e)s^2 + (b + 2cd)s + d^2}}{2GL} \quad (6)$$

p_1 requiring the negative sign

$$q = \frac{k_L a + h_L s}{L} \quad (7)$$

The theoretical amplitude ratio and phase shift can be shown (25) to be the modulus and argument respectively of the complex number resulting from the substitution of $i\omega$ for the Laplace transform parameter s in the transfer function (5).

It is interesting to note that the amplitude ratio for this model is bounded as frequency ω approaches infinity:

$$\lim_{\omega \to \infty} \left(\frac{A(Z)}{A(0)} \right) = \exp\left(-\frac{Z k_L a}{mG} \right) \quad (8)$$

The phase shift on the other hand can be shown from Equation (5) to be unbounded. That is $\lim_{\omega \to \infty} \phi = -\infty$.

The Equations for single-phase flow without absorption ($Ra = 0$) are considerably simpler. Thus Equation (2) reduces to

$$G\frac{\partial y}{\partial z} = -h_G \frac{\partial y}{\partial t} \quad (9)$$

and the transfer function becomes

$$\frac{\bar{y}(Z)}{\bar{y}(0)} = \exp\left(-\frac{Z h_G s}{G} \right) \quad (10)$$

Substitution of $s = i\omega$ in Equation (10) and reduction to the polar form of a complex number shows that the amplitude ratio for single phase slug flow is identically unity for all frequency ω. The phase shift is given by

$$\phi = -\frac{h_G Z \omega}{G} \quad (11)$$

Mixing Cell Model

In the mixing cell model the column is represented as a series of finite, perfectly-mixed longitudinal increments, or cells. This absorption mixing cell concept is an extension of a similar model for axial mixing of a single phase system first suggested by Kramers and Alberda (17).

The conservation of the liquid phase component for the nth cell yields the equation

$$x_{n+1} L - x_n L + RaH = Hh_L \frac{dx_n}{dt} \quad (12)$$

The corresponding equation for the gas phase is

$$y_{n-1} G - y_n G - RaH = Hh_G \frac{dy_n}{dt} \quad (13)$$

Laplace transformation of the preceding equations yields two finite difference equations in the transformed gas- and liquid-phase compositions. Combination of these equations with Equations (3) and (4) leads to a second-order, linear, finite difference equation in the transformed gas-phase composition $\bar{y}$:

$$T_G \bar{y}_{n+2} - (T_L T_G - fg + 1)\bar{y}_{n+1} + T_L \bar{y}_n = 0 \quad (15)$$

where

$$T_G = \frac{H h_G}{G} s + \frac{H k_L a}{Gm} + 1 \quad (16)$$

$$T_L = \frac{H h_L}{L} s + \frac{H k_L a}{L} + 1 \quad (17)$$

Solution of finite difference Equation (15) subject to the boundary conditions, $\bar{y}_n = y_o$ at $n = 0$, $\bar{x}_n = 0$ at $n = N + 1$, leads to the gas composition transfer function:

$$\frac{\bar{y}_N}{\bar{y}_o} = \frac{T_L^N \sqrt{(T_L T_G - fg + 1)^2 - 4T_L T_G}}{(T_L T_G - fg)(D_2^N - D_1^N) - T_L T_G (D_2^{N-1} - D_1^{N-1})} \quad (18)$$

where

$$D_{1,2} = \frac{(T_G T_L - fg + 1) \pm \sqrt{(T_L T_G - fg + 1)^2 - 4T_G T_L}}{2} \quad (19)$$

(D_1 requiring the negative sign)

The theoretical amplitude ratios and phase shifts were obtained from this transfer function as for the slug flow model.

The transfer function for single phase flow for the mixing cell model can be obtained from Equation (13) with $Ra = 0$:

$$\frac{\bar{y}_N}{\bar{y}_o} = \left[\frac{1}{\frac{H h_G s}{G} + 1} \right]^N \quad (20)$$

The amplitude ratio and phase shift become

$$\frac{A(Z)}{A(0)} = \left[\left(\frac{H h_G \omega}{G} \right)^2 + 1 \right]^{-\frac{N}{2}} \quad (21)$$

and

$$\phi = -N \tan^{-1}\left(\frac{H h_G \omega}{G} \right) \quad (22)$$

Axial Diffusion

In the axial diffusion model mixing along the column is described by a Fickian diffusion component in the axial direction. The concept has received wide application to mixing problems in continuous flow systems (2, 14, 16, 17, 23, 26). Equations developed from this model for the case of two phase flow are not amenable to general analytical solution and therefore will not be discussed further.

The system is considerably simplified however for single phase flow described by the differential equation

$$h_G E_G \frac{\partial^2 y}{\partial z^2} - G\frac{\partial y}{\partial z} = h_G \frac{\partial y}{\partial t} \quad (23)$$

Solution of the second-order, ordinary differential equation resulting from the Laplace transformation of Equation (22) under the boundary conditions, $\bar{y} = y(0)$ at $z = 0$; $\lim_{z \to \infty} \bar{y} = 0$, gives the transfer function of this system as

$$\frac{\bar{y}(Z)}{\bar{y}(0)} = \exp\left\{ \left(1 - \sqrt{1 + \frac{4h_G^2 E_G s}{G^2}} \right) \frac{GZ}{2h_G E_G} \right\} \quad (24)$$

Substitution of $s = i\omega$ yields a complex number which lends itself to a major simplification if $\frac{5\omega^2 E_G^2 h_G^4}{G^4} << 1$. This condition is satisfied for the conditions of the present study, and the amplitude ratio and phase shift for this single phase system become

$$\frac{A(Z)}{A(0)} \cong \exp\left(-\frac{Z E_G h_G^3 \omega^2}{G^3} \right) \quad (25)$$

$$\phi \cong -\frac{h_G Z \omega}{G}$$

It is interesting to note the similarity of the above phase shift expression for the axial diffusion model to that for the slug flow model [Equation (11)].

The mathematical details of the theoretical frequency response developments for all models of this section are presented by Gray (27).

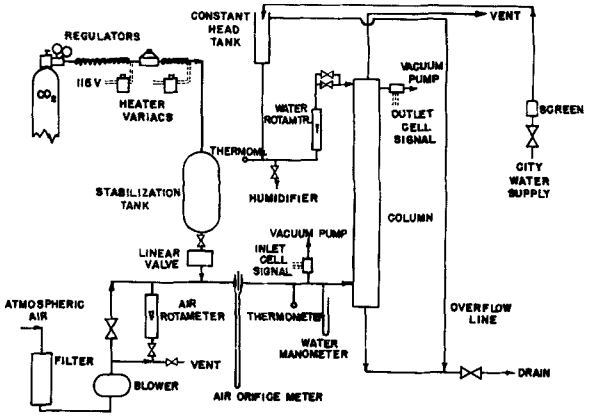

Fig. 1. Schematic diagram of column flow systems.

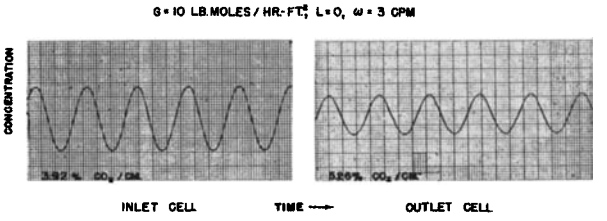

Fig. 2. Oscillograph concentration traces.

EXPERIMENTAL

Equipment

The unsteady state absorption studies were carried out in a 6-in. I.D., Pyrex glass pipe 6 ft. long, packed with ⅝-in. ceramic Raschig rings to a depth of 62 in. The packing was supported by a ¼-in. mesh stainless steel screen (free area = 87%).

Figure 1 is a schematic flow diagram of the system. Atmospheric air entered through a filter. A blower with a concentric-pulley, variable-speed drive could provide air flow rates of 0.7 to 35 cu. ft./min. at atmospheric discharge. A bypass arrangement permitted lower flows to be obtained.

USP-grade carbon dioxide was fed from cylinders to a 2,100 cu. in. stabilizer tank at 50 lb./sq. in. gauge through a two-stage pressure regulator. The lines between the regulators and to the stabilizer tank were heated by 300-v. heaters to counteract the large Joule-Thompson cooling which accompanied the continuous expansion of carbon dioxide.

The sinusoid generator consisted of a specially designed linear valve driven by a scotch yoke and variable-speed, D.C. motor. The valve flow area, provided by a sliding tongue-and-groove arrangement, was rectangular in cross section and varied directly with valve stem position. The volume flow rate was directly proportional to stem position with a constant pressure drop across the valve. The scotch yoke was driven through changeable spur gears which, in combination with the motor speed control, permitted continuous adjustment of the valve frequency from 0.1 to 15 cycles/min.

Carbon dioxide from the sinusoid generator mixed with the incoming air at a point approximately 12 in. upstream of the orifice plate. About 4½ ft. of 2-in. pipe separated the sinusoid generator and the inlet thermal conductivity cell. This pipe, which contained the orifice plate, served the dual function of creating a uniform gas mixture and filtering some of the distorting high harmonics from the original concentration sinusoid.

The carbon dioxide-air mixture entered this column through the 3-in. side of a 6- × 3-in. Pyrex reducer tee. At the top of the column the gas passed to a vent point outside the building through a 2-in. duct.

Tap water from the building supply entered the column through a constant head tank. The inlet water was distributed over the packing through a ring of ⅜-in. tubing which fed nine ⅛ in. perforated distribution tubes mounted ½ in. apart in a parallel array across the ring. The exit liquid from the column was dumped to the sewer.

The sinusoidal gas-phase concentration variations were measured by thermal conductivity cells specially designed for rapid speeds of response. High velocities of the sample and reference gases were obtained in the cells by the use of small (1/16-in. diameter) gas passages and moderately high sampling rates. Sensing elements of low heat capacity (0.014-in. diameter thermistors) were mounted immediately adjacent to the flowing stream. The time constants of these cells were found by transient tests to be 1.8 ± 0.1 sec. A complete description of the cell design is given by Gray (27). Cell temperatures were controlled by oil circulated from a constant temperature bath.

The inlet thermal conductivity cell was mounted on the gas-phase inlet pipe just at the entrance to the column. The outlet cell was supported by a 3/16 in. sample tube which passed through an aluminum flange plate on top of the column. The sampling tubes were positioned to place the sampling points at the center of the gas inlet pipe and the column.

A direct-current bridge was used in conjunction with the thermal conductivity cells for the continuous gas analysis. Variations in gas-phase composition caused unbalanced bridge signals which were detected and recorded by a low level preamplifier, driver amplifier, and single-channel oscillograph. A marking pen, activated on each cycle by a microswitch on the sinusoid generator, phased the inlet and outlet concentration sinusoids.

It was necessary to shield and ground all cell leads, bridge controls, and detecting equipment chassis.

The sampling rates were measured by capillary flowmeters, with 1½-in. sections of thermometer tubing. Four such flowmeters were used, one each for the sample and reference gas of both conductivity cells. Sample and reference gas flows were maintained by a vacuum pump and manifold arrangement. Reference gas was atmospheric air. During the absorption runs the reference air for the outlet thermal conductivity cell was passed through a small humidification column in order to match its humidity with that of the sample gas leaving the absorber.

Procedure

Prior to operation of the system the flowmeters and thermal conductivity cells were calibrated and column packing porosity was determined. Over the column operating range (0 to 20 mole % carbon dioxide) the thermal conductivity cell outputs were linear, with sensitivities of 2.55 and 2.66 mv./mole % carbon dioxide for the inlet and outlet cells respectively. The

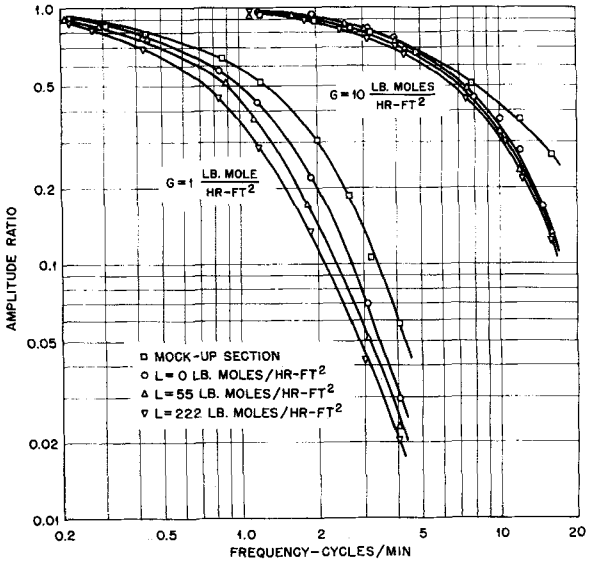

Fig. 3. Total amplitude ratio vs. frequency.

average packing porosity was 0.604. Calibration details are given by Gray (27).

The column packing was wet thoroughly prior to all gas absorption runs. Before the runs without absorption (no liquid flow) the packing was dried by blowing air through the column for several hours.

Phase flow rates were set to their desired values at the start of each run. The mean carbon dioxide concentration was then established by adjustment of the center line position of the linear valve. The amplitude of the concentration sinusoid was adjusted by varying the stroke of the scotch yoke. The sinusoid frequency was set to the desired valve with the D.C. motor speed control, and the frequency marking pen was activated. Frequencies were measured by timing the period between flashes of the oscillograph remote marker light with a stopwatch.

Inlet and outlet gas phase concentration sinusoids were recorded at six to twelve values of the sinusoid frequency for each particular set of column operating conditions. Frequency response spectra were obtained for nominal column gas phase flow rates of 1, 10, and 20 lb. moles/hr.-sq. ft. at each of two liquid phase flow rates, 55 and 222 lb. moles/hr.-sq. ft., and at zero liquid flow over dry packing.

RESULTS

Data Analysis

The dynamic response of the gas absorption system was expressed in terms of the amplitude ratio and phase shift, obtained from oscillograph concentration traces similar to those of Figure 2. Because of the placement of the thermal conductivity cells these experimental response data included not only the dynamics of the packed section but also the response of the column inlet and outlet sections and the thermal conductivity cells. The effect of these components on overall system dynamics can be evaluated from a knowledge of the frequency response of a mock-up system containing only the inlet and outlet column sections and thermal conductivity cells. At a given frequency the packing section amplitude ratio is simply the overall system amplitude ratio divided by the amplitude ratio of the mock-up system; the packing section phase shift is the difference between the overall system phase shift and the mock-up phase shift (27).

To obtain the necessary responses a full scale mock-up of the inlet and outlet sections was constructed of Pyrex pipe fittings of identical size and shape as those used in the original column installation. All features of the original system were included, except that there was no falling liquid in the inlet section. The frequency response data for the mock-up system were obtained by the same procedures used in the column absorption and nonabsorption runs. A complete frequency spectrum was obtained at gas phase flow rates as close as possible to those for the column tests.

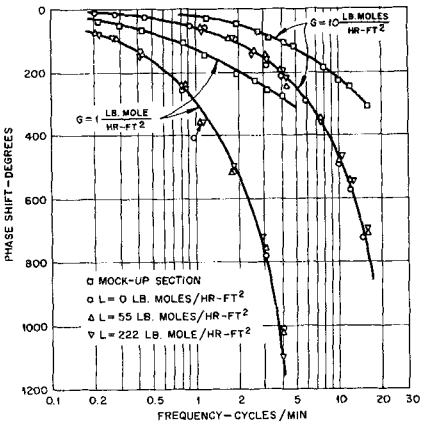

Fig. 4. Total phase shift vs. frequency.

Overall System Responses

Amplitude ratios and phase shifts for the complete system are plotted vs. the concentration sinusoid frequency ω in Figures 3 and 4. Results are shown for all gas and liquid flows employed except for runs at the nominal gas flows of 20 lb. moles/hr.-sq. ft. At this high gas flow rate the maximum frequency attainable with the sinusoid generator (15 cycles/min.) was too low to provide significant attenuation in the packing section.

A high degree of reproducibility was attained in these experiments. Amplitude ratio and phase shift curves compared for two runs made under identical conditions except for mean inlet gas-phase composition (9 mole % carbon dioxide in one case and 15 % in the other) were essentially identical.

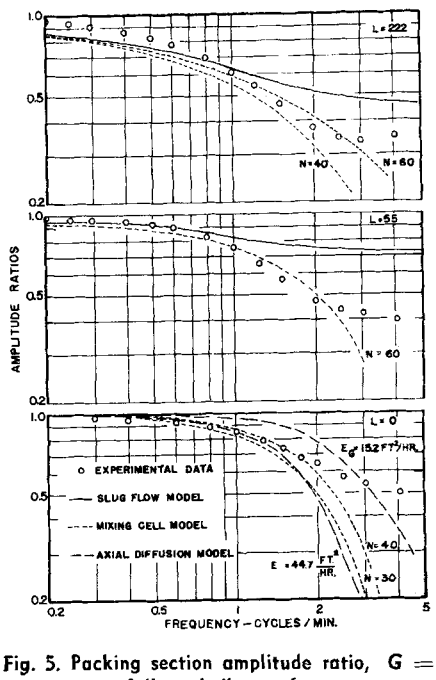

Fig. 5. Packing section amplitude ratio, G = 1 lb. mole/hr.-sq. ft.

Packing Section Responses

Figures 5 through 8 show amplitude ratios and phase shifts for the packing section alone. The circles represent experimental values, computed from the overall system response curves. The solid and dashed curves were calculated from the theoretical equations for the flow models considered (slug flow, mixing cell, and axial diffusion) for comparison with the experimental values.

Data employed in calculating the theoretical response curves were obtained as follows. Liquid phase holdups h_L were interpolated from the data of Shulman et al. (28) for 5/8-in. Raschig rings at liquid phase flow rates below loading conditions; liquid phase mass transfer coefficients k_La were taken from the results of Sherwood and Holloway (29); and the operating line slope m was computed from solubility information (30).

DISCUSSION OF RESULTS

As shown in Figures 5 and 7 the observed packing section magnitude ratios do not agree well with any of the postulated flow models at frequencies above about 1 cycle/min. At low gas flow rates the slug flow model appears to come closest to representing the experimental results but is considerably poorer at the higher gas flows. Furthermore the existence of some mixing in the packing section is strongly suggested by the marked attenuations observed in the nonabsorption ($L = 0$) runs. Here slug flow theory would predict an amplitude ratio of unity at all frequencies.

Attempts to represent the mixing phenomena by mixing cell and axial diffusion models were not satisfying. Both models yielded amplitude-ratio curves whose general shapes did not agree well with the loci of the experimental values. By proper choice of the mixing parameters (number of cells N or effective axial diffusivity E_G) agreement could be forced over rather narrow frequency ranges only. It is perhaps significant that the best fits of experimental amplitude ratios with the axial diffusion model were obtained with effective axial eddy diffusivity values consistently higher than those reported by McHenry and Wilhelm (23) and De Maria and White (22).

It is of further interest to note the similarity of the theoretical amplitude ratio responses for the axial diffusion and the mixing cell models. Thus the curve for the axial diffusion model for $E_G = 44.7$ sq. ft./hr. in Figure 5 lies

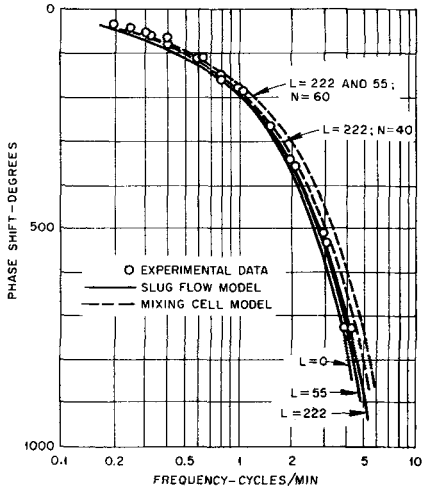

Fig. 6. Packing section phase shift, $G = 1$ lb. mole/hr.-sq. ft.

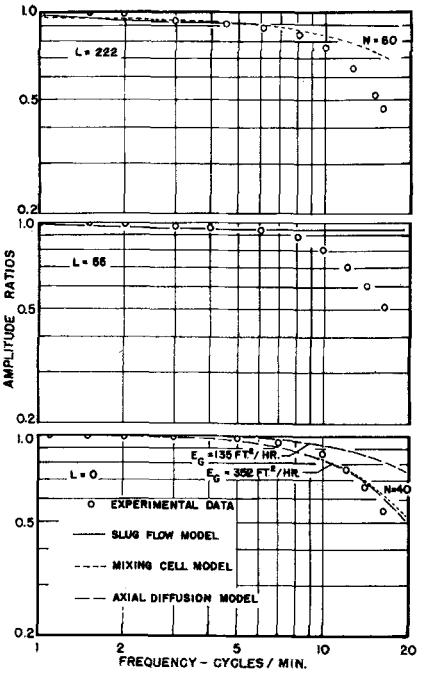

Fig. 7. Packing section amplitude ratio, $G = 10$ lb. moles/hr.-sq. ft.

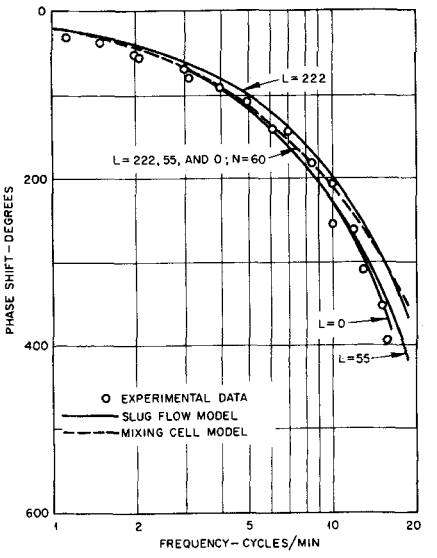

Fig. 8. Packing section phase shift, $G = 10$ lb. moles/hr.-sq. ft.

very close to that for the mixing cell model with $N = 30$. This similarity of the two models for long beds has been demonstrated from theoretical considerations by Kramers and Alberda (*17*) and by Aris and Amundson (*31*).

In contrast with the amplitude ratio results excellent agreement was obtained between theoretical and experimental phase shift curves. However these provided no basis for preferring one flow model over another, since the theoretical phase shift curves calculated for slug flow, mixing cell, and axial diffusion models were practically indistinguishable from one another. This indicates that the phase shifts are primarily determined by the mean transit time of the gas phase through the packing and are but slightly affected by moderate amounts of axial mixing.

From the above results it appears that new models, perhaps more sophisticated than the mixing cell and axial diffusion models, are needed to describe accurately the mixing phenomena in packed beds. This need has been suggested by the results of previous studies, specifically those of Kramers and Alberda (*17*), Carberry and Bretton (*19*), and De Maria and White (*22*). It is evident that the testing of models by frequency response experiments should be based on amplitude ratio measurements over a wide frequency spectrum; almost any reasonable model can be made to fit the data over a narrow frequency range, and phase shift calculations are quite insensitive to the mixing mechanism assumed.

From a practical standpoint one should realize that present models are probably adequate for describing packing section response, since a major portion of the overall system dynamics is associated with the inlet and outlet sections. This fact is demonstrated graphically in Figures 3 through 6 and emphasizes the necessity of including inlet and outlet section dynamics in any transfer function used in designing controls for packed towers. However as packing height increases, relative to the sizes of inlet and outlet sections, the effect of these sections on system dynamics should become proportionately less.

NOTATION

A = amplitude of harmonic oscillation
a = mass transfer area, sq. ft./cu. ft. packing
b = $4GL\ (h_G + h_L/m)k_La$ [Equation (6)]
c = $Gh_L - Lh_G$ [Equation (6)]
d = $(G - L/m)k_La$ [Equation (6)]
$D_{1,2}$ = quadratic roots defined in Equation (19)
e = $4GL\ h_L\ h_G$ [Equation (6)]
E_G = gas phase axial eddy diffusivity, sq. ft./hr.
f = $H\ k_La/Lm$
g = $H\ k_La/G$
G = molar mass velocity of gas phase, lb. moles/hr.-sq. ft.
$H = \dfrac{Z}{N}$ = packing height equivalent to a mixing cell, ft.
h_G = total gas phase holdup, lb. moles/cu. ft.
h_L = total liquid phase holdup, lb. moles/cu. ft.
k_L = mass transfer coefficient, lb. moles/hr.-sq. ft.-mole fraction difference
L = molar mass velocity of liquid phase, lb. moles/hr.-sq. ft.
m = slope of equilibrium line, mole fraction in vapor/mole fraction in liquid
N = number of mixing cells
$p_{1,2}$ = quadratic roots, defined in Equation (6)
q = parameter defined in Equation (7)
R = mass transfer rate, lb. moles/hr.-sq. ft. of transfer area
s = Laplace transform parameter, time^{-1}
t = time, hr.
T_G, T_L = parameters defined in Equations (16) and (17)
x = mole fraction of solute in liquid phase (deviation from steady value)
x^* = equilibrium mole fraction of solute in liquid phase (")
x_n = mole fraction of solute in liquid phase leaving nth mixing cell (")
y = mole fraction of solute in gas phase (deviation from steady value)
y_n = mole fraction of solute in gas phase leaving nth mixing cell (")
Z = total packing length, ft.
z = length dimension, ft.
ϕ = phase shift, degrees or radians
ω = angular frequency, radians/time
$\bar{\ }$ = superscript indicating Laplace transform of variable

LITERATURE CITED

1. Bilous, Olegh, and N. R. Amundson, *A.I.Ch.E. Journal*, **1**, 513 (1955); **2**, 117 (1956).

2. Cairns, E. J., and J. M. Prausnitz, *Chem. Eng. Sci.*, **12**, 20 (1960).
3. Deisler, P. F., Jr., and R. H. Wilhelm, *Ind. Eng. Chem.*, **45**, 1219 (1953).
4. "Plant and Process Dynamic Characteristics," The Society of Instrument Technology, Butterworths Scientific Publications, London, England (1957).
5. Rosenbrock, H. H., *Brit. Chem. Eng.*, **3**, 364, 432, 491 (1958).
6. Hougen, Joel O., and Robert A. Walsh, *Chem. Engr. Progr.*, **57**, 69 (1961).
7. Jaswon, M. A., and W. Smith, *Proc. Roy. Soc.*, **A225**, 226 (1954).
8. Marshall, W. R., Jr., and R. L. Pigford, "The Application of Differential Equations to Chemical Engineering Problems," p. 148, University of Delaware, Newark, Delaware (1947).
9. Bilous, Olegh, H. D. Block, and E. L. Piret, *A.I.Ch.E. Journal*, **3**, 248 (1957).
10. Fanning, R. J., and C. M. Sliepcevich, *ibid.*, **5**, 240 (1959).
11. Aikman, A. R., in "Frequency Response," p. 141, R. Oldenburger, ed., MacMillan, New York (1956).
12. Cohen, W. C., and E. F. Johnson, *Ind. Eng. Chem.*, **48**, 1031 (1956).
13. Keyes, J. J., Jr., *A.I.Ch.E. Journal*, **1**, 305 (1955).
14. Turner, G. A., *Chem. Eng. Sci.*, **10**, 14 (1959).
15. Gilbert, T. J., *ibid.*, p. 243.
16. Ebach, E. A., and R. R. White, *A.I.Ch.E. Journal*, **4**, 161 (1958).
17. Kramers, H., and G. Alberda, *Chem. Eng. Sci.*, **2**, 173 (1953).
18. Rosen, J. B., and W. E. Winsche, *J. Chem. Phys.*, **18**, 1587 (1950).
19. Carberry, J. J., and R. H. Bretton, *A.I.Ch.E. Journal*, **4**, 367 (1958).
20. Lapidus, Leon, *Ind. Eng. Chem.*, **49**, 1000 (1957).
21. Deisler, P. F., Jr., et al., *Anal. Chem.*, **27**, 1366 (1955).
22. DeMaria, Francesco, and Robert R. White, *A.I.Ch.E. Journal*, **6**, 473 (1960).
23. McHenry, K. W., Jr., and R. H. Wilhelm, *ibid.*, **3**, 83 (1957).
24. Schwartz, C. E., and J. M. Smith, *Ind. Eng. Chem.*, **45**, 1209 (1953).
25. Oldenbourg, R. C., and H. Sartorius. "The Dynamics of Automatic Controls," p. 22, The American Society of Mechanical Engineers, New York (1948).
26. Danckwerts, P. V., *Chem. Eng. Sci.*, **2**, 1 (1953).
27. Gray, Robert I., Ph.D. dissertation, The University of Tennessee, Knoxville, Tennessee (1961); Available on 35-mm. microfilm from University Microfilms, Inc., 313 N. First Street, Ann Arbor, Michigan.
28. Shulman, H. L., C. F. Ullrich, and N. Wells, *A.I.Ch.E. Journal*, **1**, 247 (1955).
29. Sherwood, T. K., and F. A. L. Holloway, *Trans. Am. Inst. Chem. Engrs.*, **36**, 39 (1940).
30. Perry, J. H., ed., "Chemical Engineer's Handbook," p. 674, McGraw-Hill, New York (1950).
31. Aris, Rutherford, and N. R. Amundson, *A.I.Ch.E. Journal*, **3**, 280 (1957).

Manuscript received January 8, 1962; revision received August 24, 1962; paper accepted August 27, 1962. Paper presented at A.I.Ch.E. New York meeting.

Burnout Conditions for Flow of Boiling Water in Vertical Rod Clusters

KURT M. BECKER

Aktiebolaget Atomenerg; Studsvik, Tystberga, Sweden

This paper deals with a new concept for predicting burnout conditions for forced convection of boiling water in fuel elements of nuclear boiling reactors.

The concept states the importance of considering the ratio of heated channel perimeter to total channel perimeter.

The perimeter ratio concept was arrived at from an experimental study of burnout conditions in rod clusters consisting of three rods of 13 mm. outside diameter and 830 mm. heated length. Data were obtained for pressures between 2.5 and 10 kg./sq. cm., surface heat fluxes between 50 and 120 W./ sq. cm., mass flow rates between 0.03 and 0.33 kg./sec., and steam qualities between 0.01 and 0.52.

The rod clearance for the experiment were 2 and 6 mm. The diameter of the channel was 41.3 mm. Additional runs were also performed after unheated displacement rods were introduced in the channel. The rod clearance in this case was 6 mm.

In the ranges investigated the measured burnout steam qualities at the outlet of the channel decrease with increasing heat flux and decreasing pressure. Furthermore it has been found that the influence of rod clearance is, in the range investigated, of small significance for engineering purposes.

It has also been observed that the present burnout steam quality data for the rod clusters are much lower than those earlier obtained for round ducts. This may be explained physically by means of the perimeter ratio concept.

It has also been found that the surface shear stress distribution around the channel perimeter and especially the position of maximum shear stress is of great importance for predicting burnout conditions for flow in channels.

Finally the new method has helped in understanding and interpreting experimental results which earlier may have seemed inconsistent.

During recent years much attention has been devoted to the problem of predicting the maximum surface heat flux which can be employed on fuel elements in pressurized or boiling nuclear reactors without danger of melting the fuel material.

The maximum heat flux is generally called the *burnout heat flux*, and the flow conditions causing burnout are defined as burnout conditions.

The thermodynamics and fluid mechanics of the phenomena causing burnout are very complicated; indeed no physical model has been established which completely explains the process and which can be used for analytical prediction of burnout heat flux. However a large number of empirical correlations based on experimental results exist. The main features of these in-